Journal of Water Process Engineering 69 (2025) 106733

Contents lists available at ScienceDirect

Journal of Water Process Engineering

journal homepage: www.elsevier.com/locate/jwpe

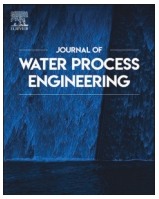

Enhanced removal and destruction of *per*- and polyfluoroalkyl substances (PFAS) mixtures by coupling magnetic modified clay and photoreductive degradation

Tao Jiang *, Md. Nahid Pervez, Aswin Kumar Ilango, Yanna Liang

Department of Environmental and Sustainable Engineering, University at Albany, State University of New York, Albany, NY 12222, USA

ARTICLE INFO

Editor: Ludovic F. Dumée

Keywords:
Per- and polyfluoroalkyl substances (PFAS)
Adsorption
Photoreductive degradation
Magnetic modified clay
Regeneration and reuse

ABSTRACT

The widespread presence of *per*- and polyfluoroalkyl substances (PFAS) in the environment poses significant challenges due to their persistence and adverse health effects. This study investigates an innovative approach to PFAS removal and destruction using a combined adsorption and photoreductive degradation system. Magnetic modified clay (MMC) was synthesized and employed as an adsorbent for six regulated PFAS, achieving high adsorption efficiencies of nearly 100 % for each PFAS. Subsequent photoreductive degradation was optimized in both reductant concentrations and pH to enhance PFAS breakdown under the 285 nm UV light. The study demonstrated the potential of MMC to effectively adsorb PFAS and facilitate their degradation through a photochemical process, achieving substantial defluorination efficiency. Under optimal photodegradation conditions with 50 mM Na_2SO_3 and 10 mM KI at pH 12, the overall defluorination efficiency reached 66.5 ± 1.1 % after 48 h. Regeneration and reuse of MMC were also evaluated, showing promising results for the sustainable treatment of PFAS-contaminated water. This combined approach offers a cost-effective and environmentally friendly solution for mitigating PFAS pollution.

1. Introduction

A wide variety of synthetic organic compounds with fluorinated carbon backbones are collectively known as *per*- and polyfluoroalkyl substances (PFAS). Because of their unique properties, PFAS have found widespread use in a various range of industrial processes and consumer products, including but not limited to surfactants in oil and mining [1,2], coatings for clothing and food packaging [3,4], foams for the production of aqueous films [5,6], personal care products [7], cleaning agents [8], and a plethora of other uses [9]. PFAS, which have been manufactured for over six decades and are now commonly found, are acknowledged as presenting significant hazards to human health and the environment [10,11]. Therefore, it is crucial to prioritize the development of inventive methods to eliminate PFAS from the environment.

Various methods have been investigated for the treatment of PFAS, including physical adsorption/filtration, chemical/electrochemical destruction, and biological degradation [12]. Adsorption stands out as one of the most promising approaches to eliminating PFAS from water sources due to its ease of application, cheap cost, and high removal efficacy. To date, researchers have investigated many substances that may adsorb PFAS, such as carbon-based materials [11,13,14], ion exchange resins [15,16], biosorbents [17–20], and clay-based materials [21,22]. Nevertheless, most of these adsorbents have significant limitations in capturing a broad range of short- and long-chain PFAS, as well as challenges in material regeneration. For example, it is extremely challenging to reduce the concentration of short-chain PFAS in water to single-digit ng/L levels cost-effectively using granular activated carbon (GAC) [23]. In terms of regeneration, although different approaches have been reported, such as chemical, electrochemical and ultrasound [24–26], thermal regeneration remains as the most promising [27]. This thermal process, however, is highly energy-intensive.

In recent years, photocatalytic degradation has gained popularity for breaking down PFAS due to its relatively inexpensive energy needs and high transformation efficiency [28,29]. Photodegradation can be divided into photooxidation and photoreduction. PFAS undergo oxidative degradation by undergoing one electron transfer to reactive species generated by photocatalysts, resulting in the detachment of functional groups and the shortening of the carbon chain. Prior research has recorded the breakdown of PFAS by photooxidation when exposed to UV or visible light in the presence of semiconductor photocatalysts, such as

* Corresponding author.
E-mail address: tjiang2@albany.edu (T. Jiang).

https://doi.org/10.1016/j.jwpe.2024.106733
Received 29 August 2024; Received in revised form 3 December 2024; Accepted 4 December 2024
Available online 7 December 2024
2214-7144/© 2024 Elsevier Ltd. All rights are reserved, including those for text and data mining, AI training, and similar technologies.

TiO_2 and Ga_2O_3 [30,31]. Within this system, the breakdown of PFAS is thought to be associated with photogenerated holes (h^+_{vb}) that possess a potent oxidation capability. The general oxidation pathways of perfluorocarboxylic acids (PFCAs; $C_nF_{2n+1}COO^-$) may be characterized by the acid transforming into an unstable $C_nF_{2n+1}COO^\bullet$ radical, which then undergoes decarboxylation to form a perfluoroalkyl radical $C_nF_{2n+1}^\bullet$ [32,33]. During liquid-phase photocatalytic reactions, the hydroxyl radical ($HO^\bullet$) is produced by splitting water when exposed to UV or visible light [34]. This $HO^\bullet$ then combines with the perfluoroalkyl radical to create $C_nF_{2n+1}OH$ in the water. However, $HO^\bullet$ is unable to break down PFCAs like perfluorooctanoic acid (PFOA) for two reasons. Firstly, the carbon chain of PFCAs does not have any hydrogen atoms that can be removed [35]. Secondly, the oxidation potential of $HO^\bullet$ is lower than the average energy required to break a C—C bond, which is 276.0 kJ/mol compared to 347.0 kJ/mol [36].

Recently, UV photochemical reactions that produce hydrated electrons (e^-_{aq}) have been recognized for their ability to effectively degrade both PFCAs and perfluorosulfonic acids (PFSAs) [37]. While several photosensitizers and inorganic anions such as dithionite have been employed to enhance the efficiency of e^-_{aq} toward the breakdown of PFAS, I^- and SO_3^{2-} are the most often used [38,39]. The generation of e^-_{aq} in the UV/I^- system occurs via the photoexcitation of I^-, forming an excited iodide species ($I^\bullet H_2O^{-*}$) [40,41]. This species then undergoes a transformation into a caged complex ($I^\bullet$, e^-) consisting of an iodine atom and an electron, or it may decay back to the ground state (I^-). The caged complex dissociates, producing e^-_{aq} [40]. The iodine atom produced in this process undergoes further reactions with I^-, resulting in the formation of many additional iodine species that have the ability to consume e^-_{aq} [42,43]. $SO_3^\bullet$ and e^-_{aq} may be generated in a UV/SO_3^{2-} system that is operated under alkaline conditions [44,45]. In a recent study, the researchers discovered that the presence of I^- ions greatly speeds up the breakdown of PFSAs and PFCAs in the UV/SO_3^{2-} aqueous system (UV/SO_3^{2-} + I^-) [46,47]. This is due to the higher concentration of e^-_{aq} and greater consumption of SO_3^{2-} ions, resulting in improved degradation. Additionally, the authors noted that the use of power and chemicals in the UV/SO_3^{2-} + I^- system was much less compared to the UV/SO_3^{2-} system while removing an equivalent quantity of PFSAs or PFCAs [48,49].

These encouraging results inspired us to hypothesize that the UV/SO_3^{2-} + I^- system is able to destroy PFAS in spent adsorbent and thus leads to regeneration and reuse of the adsorption material. To test this hypothesis, we chose magnetic modified clay (MMC) made from inexpensive clay minerals [22]. Magnetic adsorbents are highly valued for their unique adsorption properties and ease of separation in water under a magnetic field [50,51]. Our earlier investigation indicated that MMC exhibited higher PFAS adsorption performance than that of commonly used commercial adsorbents [22]. In the context of snowmelt treatment, MMC outperforms powdered activated carbon (PAC) in PFAS removal efficiency. Specifically, at initial concentrations of 1 μg/L for C6-C8 PFCAs; C4, C6, and C8 PFSAs; and undecafluoro-2-methyl-3-oxahexanoic acid (GenX), MMC achieved removal efficiencies of 84–100 % over 8 h, exceeding the performance of PAC, which ranged from 68 to 95 %. Additionally, its magnetic separation feature allows fast and easy adsorbent harvesting and prevents potential secondary contamination. Taking advantage of these benefits, MMC might be an important advancement for PFAS removal from water via a combined adsorption and degrading strategy. This would address the limitations of conventional adsorbents, such as GAC which requires intensive energy for regeneration. Thus, this work was designed to addresses these questions: (i) what condition can lead to maximum degradation of PFAS in spent MMC? and (ii) can the spent MMC after photoreduction be reused?

2. Materials and methods

2.1. Chemical reagents

The six regulated PFAS tested in the adsorption and photodegradation experiments, i.e., perfluorobutane sulfonate (PFBS), GenX, perfluorohexane sulfonate (PFHxS), perfluorooctane sulfonate (PFOS), PFOA, and perfluorononanoic acid (PFNA), along with additional PFAS for reusability adsorption experiments and transformation product determination, such as trifluoroacetic acid (TFA; C2), pentafluoropropionic acid (PFPrA; C3), perfluorobutanoic acid (PFBA; C4), perfluoropentanoic acid (PFPeA; C5), perfluorohexanoic acid (PFHxA; C6), and perfluoroheptanoic acid (PFHpA; C7), were purchased from various suppliers listed in Table S1. Chemicals used in photochemical degradation experiments, including sodium sulfite (Na_2SO_3), potassium iodide (KI), sodium bicarbonate ($NaHCO_3$), and sodium hydroxide (NaOH), were obtained from Fisher Scientific (Waltham, MA, USA). Detailed information about all chemicals used in this study is listed in Table S1.

2.2. Synthesis of magnetic modified clay

The procedure for preparing magnetic modified clay (MMC) is detailed in a previous publication [22]. Briefly, modified clay (MC) was first synthesized from montmorillonite following a two-step process described by Jiang et al. [21]. The MC was then reacted with $FeCl_3{\cdot}6H_2O$ and $FeCl_2{\cdot}4H_2O$ with a mass ratio of 2.9:2.74:1 at 90 °C under a pH of ca. 10 for 1 h. The resulting MMC was collected, rinsed, and dried for future use. In the composition of MMC, the mass ratio of montmorillonite to manganite is approximately 0.7:1.

2.3. Adsorption experiments

The adsorption experiments with MMC were conducted using mixtures containing the six regulated PFAS. To generate sufficient quantities of PFAS-laden MMC for photodegradation experiments, the MMC dose in adsorption was 2 g/L, and the initial concentration of each PFAS was approximately 1 mg/L. The mixtures were agitated at 150 rpm at room temperature for 48 h to reach adsorption equilibrium [22]. Following this, the MMC was collected by centrifugation, and the PFAS in the supernatant were determined using an Agilent Technologies 1290 Infinity II LC system paired with a 6470 Triple Quad Mass Spectrometer (LC-MS/MS, Santa Clara, CA, USA). Additionally, individual adsorption experiments were performed for three PFAS, i.e., GenX, PFOA, and PFOS, with initial concentrations of 5.17, 5.62, and 6.62 mg/L, respectively. All other experimental conditions remained the same as those in the PFAS mixture adsorption experiments.

After reaching the equilibrium of adsorption, the spent MMC with adsorbed PFAS was subjected to UV irradiation for photoreductive degradation. After photodegradation, a portion of the residual MMC with adsorbed PFAS mixtures was rinsed by deionized (DI) water and subject to further adsorption experiments to assess the reusability of regenerated MMC. A total of three photodegradation-adsorption cycles were conducted to evaluate the durability and performance of the regenerated MMC. In these adsorption experiments, a PFAS mixture including PFOA, PFNA, PFDA, perfluoroundecanoic acid (PFUnA), PFOS, 6:2 FTSA, and 2-N-ethyl perfluorooctane sulfonamido acetic acid (N-EtFOSAA), each at a starting concentration of 10 μg/L, was used with an adsorbent dose of 100 mg/L. Subsamples were collected for PFAS analysis at six time points, i.e., 0, 1, 4, 8, 24, and 48 h. These conditions were commonly applied in previous adsorption studies [21,22].

2.4. Photochemical degradation experiments

Photodegradation experiments were conducted with PFAS-laden MMC in 250-mL high-density polyethylene cylinders wrapped in

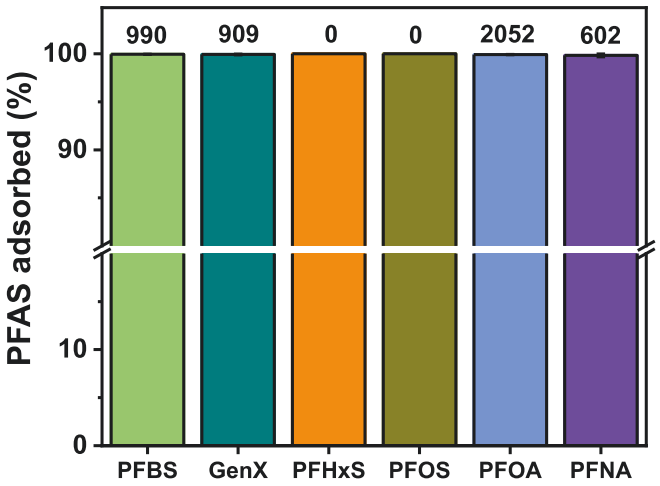

Fig. 1. Adsorption of the six regulated PFAS by magnetic modified clay after 48 h. The initial concentration of each tested PFAS was around 1.2 mg/L, and the MMC dose was 2 g/L (0.1 g in 50 mL). The PFAS solution pH was unadjusted. Error bars represent the standard deviations of triplicate tests. The numbers above each bar are the residual PFAS concentrations in ng/L, and zero indicates a residual concentration lower than the limit of detection for each PFAS shown in Table S2.

aluminum foil. A 10 W low-pressure mercury 254-nm ultraviolet lamp (GPH212T5L/4P, Light Spectrum Enterprises Inc., USA) in a quartz sleeve was placed vertically in each cylinder, irradiating 80 mL of aqueous solutions containing 5 mM $NaHCO_3$ and predetermined concentrations of Na_2SO_3 and KI. The initial pH was set to 12 with 1 M NaOH and either maintained or left uncontrolled. Solution temperature was kept at ~20 °C with a circulated cooling system, and the mixture was stirred at 450 rpm during photodegradation with MMC.

Aqueous samples were collected and centrifuged at predetermined intervals. The supernatant samples were subject to analysis of fluoride ion (F^-) and PFAS. The pellet left after the centrifugation was returned to the corresponding cylinder system. At the conclusion of the experiments, residual MMC and the aqueous phase were separated by centrifugation for further treatment and analysis. The remaining PFAS and F^- in the residual MMC were extracted through three rounds of methanol extraction with 0.1 M ammonium hydroxide. The basic methanol extract was then analyzed for PFAS and F^- content. The overall defluorination efficiency (deF%) was calculated as (Eq. (1)):

$$\text{deF\%} = \frac{C_{F^-}}{C_0 \times N_F} \times 100\% \quad (1)$$

where C_F^- is the molar concentration of F^- in the solution and rinsate derived from the three rounds of methanol extraction of the residual MMC, C_0 is the initial molar concentration of the parent PFAS, and N_F is the number of F in the parent PFAS molecule. Statistical analyses for deF % and F mass across different groups were conducted using the Student's *t*-test ($p < 0.05$ indicates statistically significant difference).

2.5. Chemical analysis

Parent PFAS and transformation products (TPs) in the collected supernatant samples and methanol extracts were quantified using the

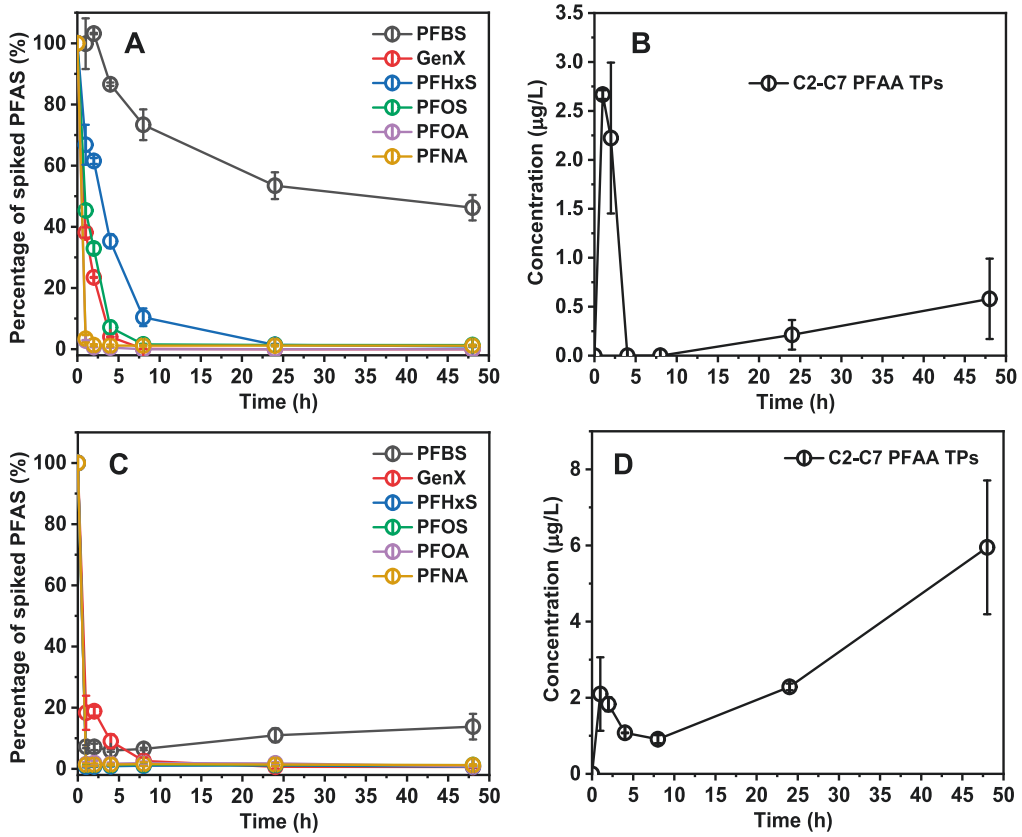

Fig. 2. Photodegradation of PFAS in aqueous solutions without (A and B) and with (C and D) pristine magnetic modified clay. (A and C) The changes in percentage of spiked concentration (%) of each parent PFAS. (B and D) Total concentrations (μg/L) of C2-C7 PFAA transformation products. The initial concentrations of the parent PFAS were around 0.8–1.0 mg/L, and the pristine MMC doses in (C) and (D) were 2.5 g/L (0.2 g in 80 mL). Photodegradation conditions were: 50 mM Na_2SO_3, 10 mM KI, and 5 mM $NaHCO_3$ at the initial pH of 12 (uncontrolled throughout the experiments) and around 20 °C. Error bars represent the standard deviations of duplicate tests.

Agilent LC-MS/MS. The analysis focused on perfluoroalkyl acids (PFAAs) as the TPs. Prior to analysis, samples were spiked with ^{13}C-PFOS and ^{13}C-PFOA as internal standards. The quantification methods for PFAS using LC-MS/MS are detailed in previous reports [52–55] and are provided in Text S1 and Tables S2 and S3.

The non-extractable total fluorine content, including organofluorine and inorganic fluorine in the residual MMC after methanol extraction, was analyzed using a combustion ion chromatography (CIC) system, consisting of a combustion module with an Auto Boat Drive (ABD) and a 930 Compact IC Flex instrument (Metrohm, Herisau, Switzerland) equipped with a conductivity detector. A Metrosep SUPP 5 column (Metrohm) was used for the separation of anions. The eluent for the elution process was a carbonate buffer consisting of 1.8 mM Na_2CO_3 and 1.7 mM $NaHCO_3$ (1:1) with a flow rate of 0.7 mL/min. To mitigate conductivity, a solution of 0.05 M H_2SO_4 was used as a regenerating agent. Calibration samples were prepared using a PFOA standard dissolved in methanol [56]. The F^- in the aqueous phase were measured using a Thermo Scientific Orion Dual Star two-channel pH/ISE meter with a 9609BNWP Sure-Flow fluoride ion-selective electrode (Waltham, MA, USA). Standards were prepared from a NaF standard solution in DI water.

3. Results and discussion

3.1. PFAS adsorption by magnetic modified clay

Prior to the photodegradation of PFAS adsorbed onto MMC, the adsorption of six different regulated PFAS was performed with MMC. According to Fig. 1, all PFAS were captured with about 100 % removal efficiency at an initial individual concentration of ca. 1.2 mg/L, and no desorption was seen over the 48-h exposure. These results demonstrated that MMC had superior adsorption capabilities for both long- and short-chain PFAS similar to MC we reported already [21] and the MMC tested with PFAS at μg/L or ng/L concentrations [22]. This provided strong evidence that MMC has the potential to be an excellent PFAS adsorbent in water.

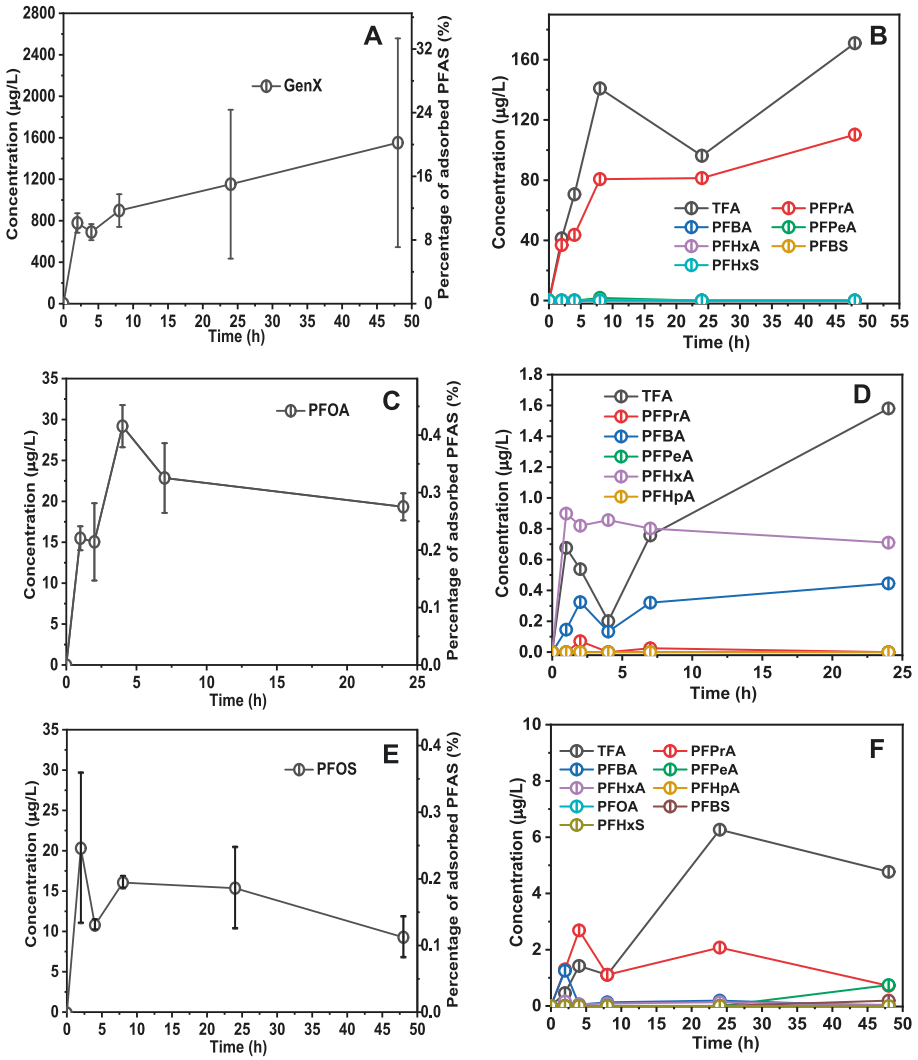

Fig. 3. Photodegradation of PFAS in aqueous solutions with the spent magnetic modified clay adsorbed with individual GenX (A and B), PFOA (C and D), and PFOS (E and F). (A, C, and E) The changes in concentration (μg/L; left Y-axis) and percentage of adsorbed concentration (%; right Y-axis) in photodegradation. (B, D, and F) Concentration (μg/L) of each PFAA transformation product. Photodegradation was conducted after adsorption. The initial adsorbed masses of GenX, PFOA, and PFOS in the spent MMC were 3.07, 2.81, and 3.30 mg/g, respectively. All the doses of the spent MMC in the three aqueous solutions in photodegradation were 2.5 g/L (0.2 g in 80 mL). Photodegradation conditions were: 10 mM Na_2SO_3, 2 mM KI, and 5 mM $NaHCO_3$ at the initial pH of 12 (uncontrolled throughout the experiments) and around 20 °C. Error bars represent the standard deviations of duplicate tests.

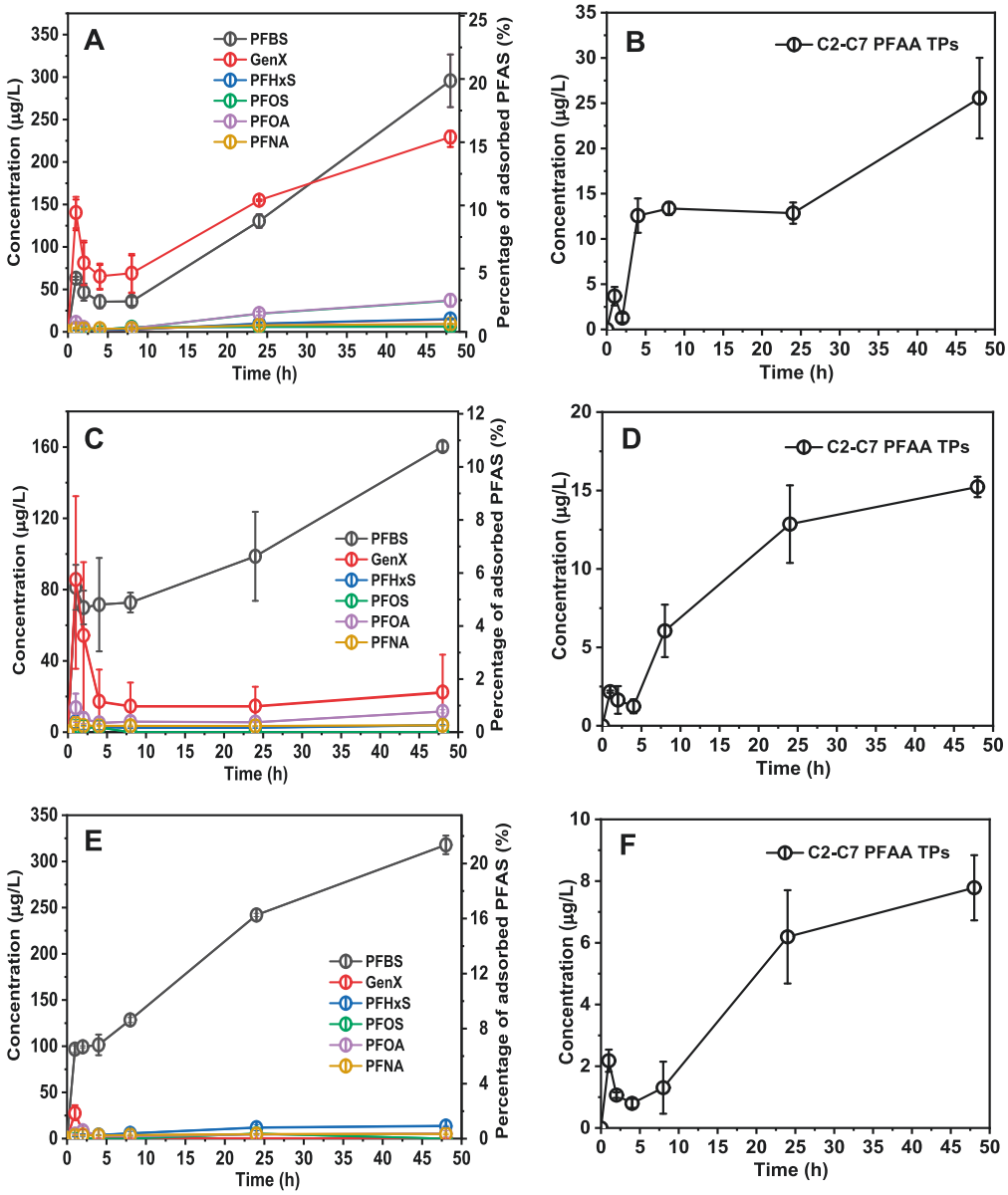

Fig. 4. Photoreductive degradation of adsorbed PFAS in the spent MMC at various reductant concentrations: (A and B) 10 mM Na_2SO_3 and 2 mM KI, (C and D) 20 mM Na_2SO_3 and 4 mM KI, (E and F) 50 mM Na_2SO_3 and 10 mM KI. (A, C, and E) The changes in concentration (μg/L; left Y-axis) and percentage of adsorbed concentration (%; right Y-axis) in photodegradation. (B, D, and F) Total concentrations (μg/L) of C2-C7 PFAA transformation products. Photodegradation was conducted after adsorption. The total initial adsorbed mass of PFAS was 3.64 mg/g, with each PFAS accounting for approximately the same amount. The spent MMC dose in aqueous solution was 2.5 g/L (0.2 g in 80 mL). Other chemical reagent and conditions for all groups were: 5 mM $NaHCO_3$ at the initial pH of 12 (uncontrolled throughout the experiments) and around 20 °C. Error bars represent the standard deviations of duplicate tests.

3.2. Photochemical degradation of PFAS in aqueous solutions with and without pristine magnetic modified clay

The efficiency for photoreductive degradation of the six regulated PFAS in aqueous solutions both in the absence and presence of pristine MMC was evaluated. One of the aims was also to validate the photodegradation of the parent PFAS under reductive conditions with Na_2SO_3 and KI. The C2-C7 PFAAs were selected as the primary TPs during the photodegradation. The rationale for focusing on these shorter-chain PFAAs as TPs was grounded in the well-documented degradation pathways of long-chain PFAS under reductive conditions, particularly those involving e^-_{aq} generated in UV/sulfite systems. It has been demonstrated that during reductive defluorination of PFAS, the breakdown of the parent molecules typically involved sequential cleavage of the terminal CF_2 groups, resulting in the stepwise formation of shorter-chain PFAAs (e.g., C2-C7) as stable intermediates [29]. The chain-length distribution of these TPs reflected the progressive defluorination and carbon chain shortening process characteristic of advanced reduction treatments [44]. However, it is important to acknowledge the limitations in detecting only these shorter-chain PFAAs as TPs. It has been shown that the complexity of PFAS degradation can lead to the formation of a wide variety of partially defluorinated intermediates and byproducts, some of which may not be fully captured in the analysis of C2-C7 PFAAs alone [57]. While C2-C7 PFAAs may not encompass all TPs formed during the process, they can still serve as useful indicators of degradation.

Fig. 2 illustrates the degradation trends for the six parent PFAS and the total formation of C2-C7 PFAAs as TPs under conditions of 50 mM Na_2SO_3 and 10 mM KI. Without MMC, a noticeable decrease in the concentration of all six parent PFAS was observed (Figs. 2A and S1A), indicating their effective breakdown over the photodegradation period.

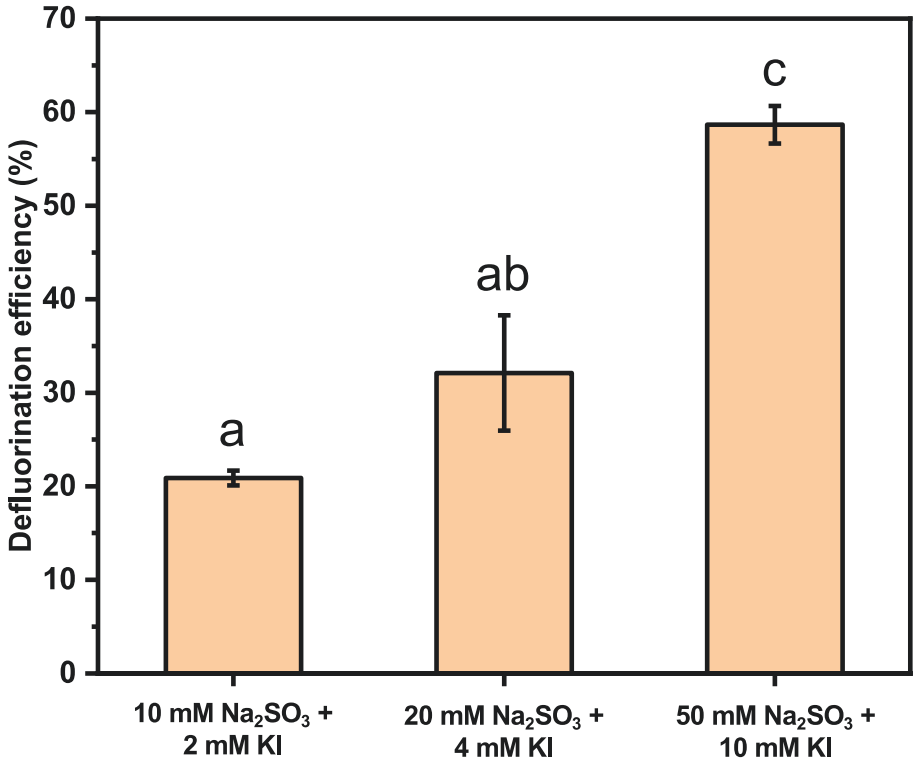

Fig. 5. Overall defluorination efficiency (%) in the photodegradation of adsorbed PFAS in the spent MMC at various reductant concentrations: 10 mM Na_2SO_3 and 2 mM KI, 20 mM Na_2SO_3 and 4 mM KI, and 50 mM Na_2SO_3 and 10 mM KI. The total initial adsorbed mass of PFAS was 3.64 mg/g, with each PFAS accounting for approximately the same amount. The spent MMC dose in aqueous solution was 2.5 g/L (0.2 g in 80 mL). Other chemical reagent and conditions for all groups were: 5 mM $NaHCO_3$ at the initial pH of 12 (uncontrolled throughout the experiments) and around 20 °C. Error bars represent the standard deviations of duplicate tests. Different letters above the bars represent significant differences among various groups ($p < 0.05$).

This was further supported by the high deF% and decay efficiency of pure PFOA and PFOS in solutions, with deF% of 96.0 ± 1.0 % and 99.4 ± 0.7 %, respectively (Fig. S2). However, the photodegradation rates varied among the different PFAS. The short-chained PFBS showed the slowest degradation rate, with the remaining percentage of 46.3 ± 4.2 % at the end of experiment (48 h) (Fig. 2A). Previous research also demonstrated that PFBS was the most difficult to decay among the six regulated PFAS [29] because of its shorter carbon chain length, robust molecular structure, and higher chemical stability. All other five PFAS exhibited much higher degradation rates, especially within the initial 2 h, achieving nearly 100 % decay efficiency at 48 h. Fig. 2B details the total concentrations of C2-C7 PFAA TPs formed during the photodegradation process. The formation of total by-products increased over the initial 2 h, sharply decreased to zero at 4–8 h, and increased slowly again until 48 h (Fig. S1B). This trend may be due to the very high degradation rates of the parent PFAS and the slower breakdown of the shorter-chain TPs at the initial time, leading to the accumulation of TPs in the beginning.

Previous studies have demonstrated that the use of montmorillonite clays, particularly organo-modified variants, can enhance the photodegradation of PFAS due to their ability to stabilize and extend the persistence of the reactive species (e.g., e_{aq}^-) generated during the process. For instance, montmorillonite modified with hexadecyltrimethyl ammonium (HDTMA) has been shown to adopt a tilted conformation within the clay interlayers, which effectively isolated and shielded e_{aq}^- from quenching by oxygen [58]. This protection promoted the defluorination of PFOA under UV irradiation. In contrast, in our study, the use of MMC did not lead to the same enhancement in PFAS degradation. The results from Figs. 2 and S1 indicated that the presence of pristine MMC led to high removal efficiency of PFAS in aqueous solutions. However, the removal included photodegradation and adsorption. The further analysis of defluorination revealed that in the presence of pristine MMC, the deF% was 18.5 ± 0.2 % at the end of experiment, compared to 79.6 ± 1.4 % for the PFAS mixture solution without MMC. This suggested that MMC may inhibit the photodegradation process, possibly due to the adsorption of PFAS onto the pristine MMC, which reduced their availability for photodegradation compared to the PFAS mixture solution. The lower deF% in the presence of MMC was not contradictory with the increased TPs, as these intermediates tended to accumulate rather than fully break down into individual C, O, and F atoms, resulting in lower overall defluorination. The discrepancy between our findings and previous studies indicates that the specific modifications and the nature of the clay material play critical roles in influencing the efficiency of photochemical processes. The interlayer spacing, surface chemistry, and presence of magnetite within MMC layers likely differ from organo-modified clays [22,58], which could affect the interaction between the clay and PFAS molecules, as well as the generation and stabilization of reactive species. The magnetite component in MMC may contribute additional adsorption sites and alter electrostatic interactions, potentially enhancing PFAS retention within the clay structure. This enhanced adsorption could limit PFAS exposure to reactive species, reducing their availability for photodegradation, which could partially explain the observed lower deF% in the presence of pristine MMC.

3.3. Destruction of adsorbed PFAS in MMC by photochemical degradation

The photochemical degradation of PFAS adsorbed onto MMC was systematically investigated under various conditions. Fig. 3 illustrates the changes in concentration and percentage of adsorbed GenX, PFOA, and PFOS individually, as well as their TPs, during photodegradation with 10 mM Na_2SO_3 and 2 mM KI at an initial pH of 12. The initial adsorbed masses of GenX, PFOA, and PFOS in MMC were 3.07, 2.81, and

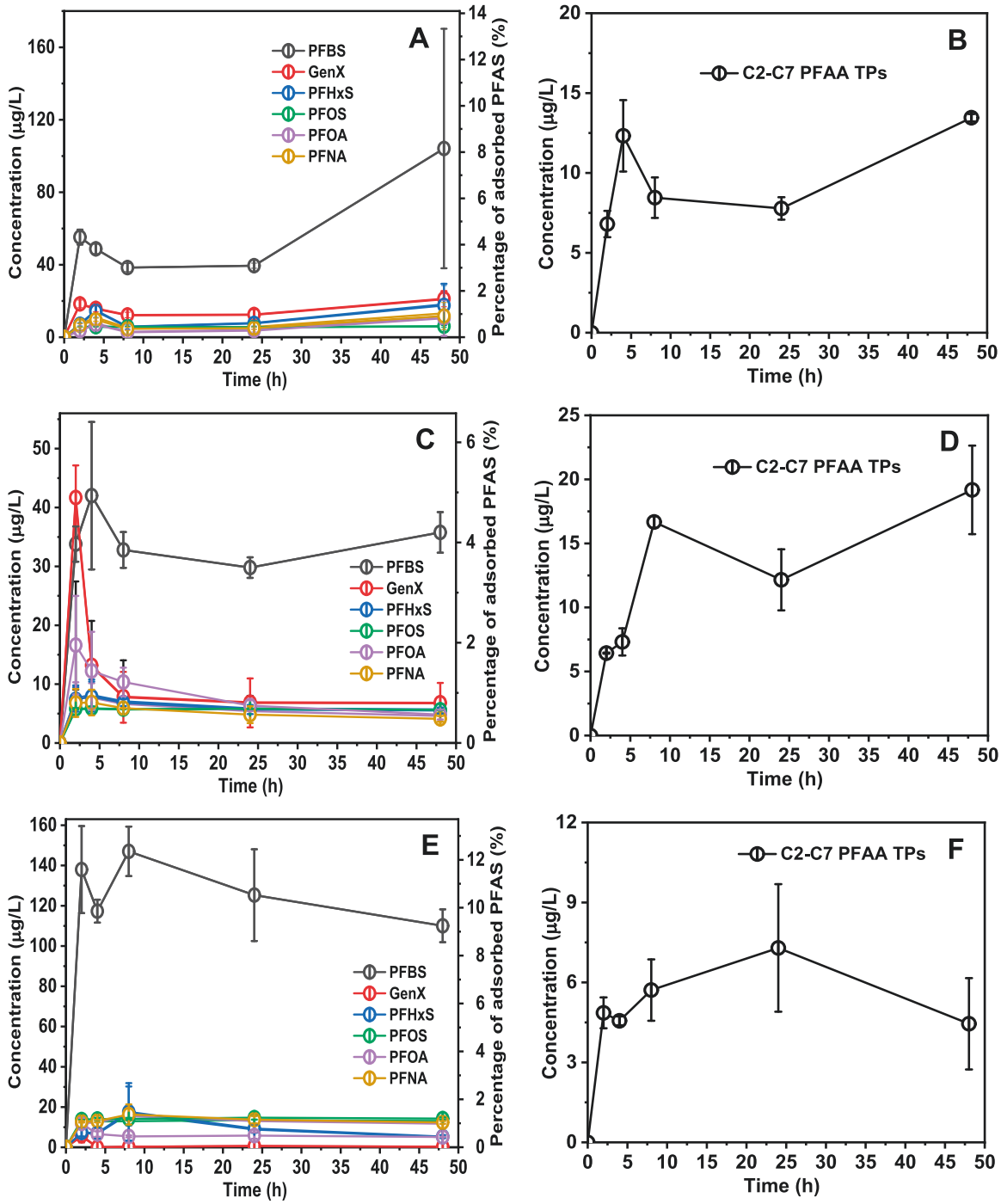

Fig. 6. Photoreductive degradation of adsorbed PFAS in the spent MMC at various conditions: (A and B) 100 mM Na_2SO_3 and 20 mM KI at initial pH 12 (uncontrolled), (C and D) 50 mM Na_2SO_3 and 10 mM KI at stable pH 12, (E and F) 100 mM Na_2SO_3 and 20 mM KI at stable pH 12. (A, C, and E) The changes in concentration (μg/L; left Y-axis) and percentage of adsorbed concentration (%; right Y-axis) in photodegradation. (B, D, and F) Total concentrations (μg/L) of C2-C7 PFAA transformation products. Photodegradation was conducted after adsorption. The total initial adsorbed mass of PFAS was 3.1 mg/g, with each PFAS accounting for approximately the same amount. The spent MMC dose in aqueous solution was 2.5 g/L (0.2 g in 80 mL). Other chemical reagent and conditions for all groups were: 5 mM $NaHCO_3$ at around 20 °C. Error bars represent the standard deviations of duplicate tests.

3.30 mg/g, respectively, with MMC doses of 2.5 g/L. For all three PFAS, the concentrations in the aqueous phase showed a rapid initial increase, with GenX exhibiting a higher aqueous concentration than PFOA and PFOS (Fig. 3A, C, and E). This indicated that GenX was desorbed more readily, resulting in significantly higher levels of TPs (Fig. 3B, D, and F).

Regarding the defluorination efficiency for GenX, PFOA, and PFOS when adsorbed onto MMC, GenX exhibited the highest defluorination efficiency of 66.3 ± 18.0 %, followed by PFOA with 42.2 ± 1.5 % and then PFOS with 26.7 ± 1.9 % (Fig. S3). However, this did not necessarily indicate that GenX was more readily photodegraded. Previous research has shown that GenX was actually more recalcitrant to decay compared to PFOA and PFOS [59,60]. The higher defluorination percentage of GenX observed in our study could be attributed to its greater tendency to desorb, resulting in higher aqueous concentrations of GenX available for photodegradation compared to PFOA and PFOS (Fig. S4). The lower deF % of PFOA and PFOS may be attributed to the stronger interactions of

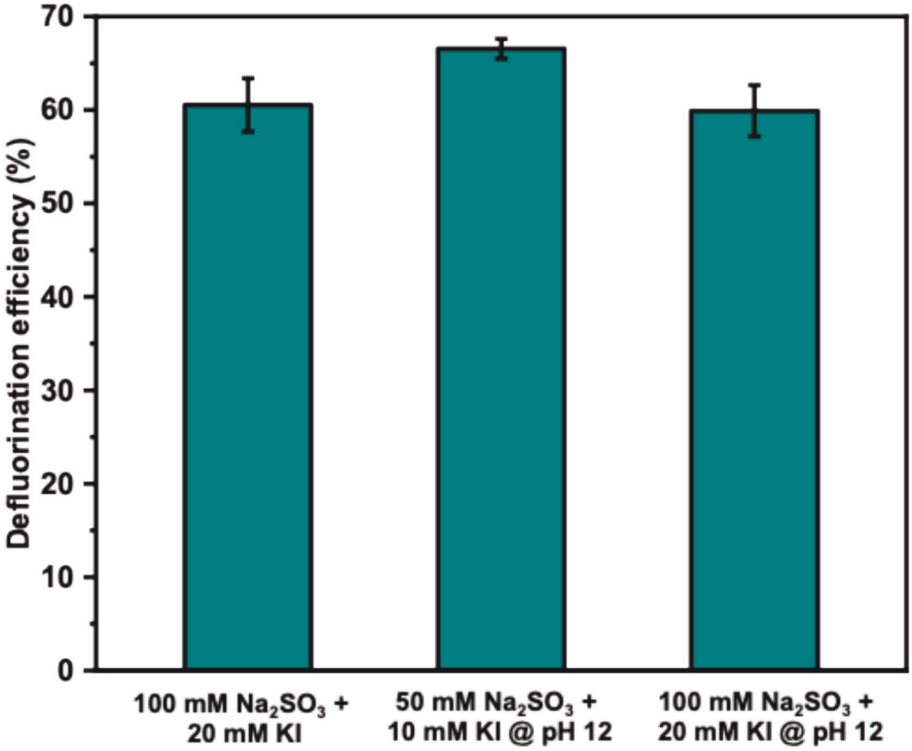

Fig. 7. Overall defluorination efficiency (%) in the photodegradation of adsorbed PFAS in the spent MMC at various conditions: 100 mM Na_2SO_3 and 20 mM KI at initial pH 12 (uncontrolled), 50 mM Na_2SO_3 and 10 mM KI at stable pH 12, and 100 mM Na_2SO_3 and 20 mM KI at stable pH 12. The total initial adsorbed mass of PFAS was 3.1 mg/g, with each PFAS accounting for approximately the same amount. The spent MMC dose in aqueous solution was 2.5 g/L (0.2 g in 80 mL). Other chemical reagent and conditions for all groups were: 5 mM $NaHCO_3$ at around 20 °C. Error bars represent the standard deviations of duplicate tests. Statistical analyses showed no significant differences of deF% among various groups.

PFOA and PFOS with the MMC compared to GenX (Fig. S4), which could also enhance their resistance to photochemical decay. The stronger binding of PFOA and PFOS to MMC could result in a higher proportion of these compounds being retained and subsequently degraded within the MMC matrix, compared to the more readily desorbed GenX. This finding highlights the complex interplay between adsorption characteristics and photodegradation efficiency for different PFAS compounds.

The influence of different reductant concentrations on the photoreductive degradation of adsorbed PFAS mixtures in MMC was also examined, as shown in Figs. 4 and 5. Three sets of reductant concentrations were tested: 10 mM Na_2SO_3 and 2 mM KI, 20 mM Na_2SO_3 and 4 mM KI, and 50 mM Na_2SO_3 and 10 mM KI. The total initially adsorbed mass of six PFAS was 3.64 mg/g, with each PFAS accounting for approximately the same amount. The results showed higher reductant concentrations led to lower PFAS in aqueous phase, except for PFBS (Fig. 4A, C, and E). This trend suggested that increasing the availability of reductants enhanced the generation of reactive species, thereby accelerating the photodegradation process. Additionally, the lower total concentrations of C2-C7 PFAA TPs, as well as each TP, were observed at higher reductant concentrations (Figs. 4B, D, F, and S5), indicating that higher doses of Na_2SO_3 and KI facilitated the more extensive breakdown of both parent and daughter PFAS molecules.

Fig. 5 summarizes the overall defluorination efficiency for each parent PFAS at the three reductant concentrations tested. The results confirmed that increasing the concentration of reductants enhanced the overall deF%, with the highest concentrations (50 mM Na_2SO_3 and 10 mM KI) achieving the most effective PFAS destruction. As the reductant concentrations increased, the overall deF% rose from 20.9 ± 0.8 %, to 32.1 ± 6.2 %, and to 58.7 ± 2.0 %, respectively. The enhanced deF% at higher reductant concentrations can be attributed to the increased production of reactive species, which facilitates the breakdown of PFAS molecules. This was consistent with the above results indicating that higher concentrations of reductants improved the photoreductive degradation efficiency.

3.4. Optimization of conditions for photochemical degradation

Besides the reductant concentrations, pH was also found to be influential on the photoreductive degradation of PFAS [44,47]. Thus, different concentrations of Na_2SO_3 and KI, as well as the impact of pH control on the photochemical degradation of PFAS adsorbed on MMC was investigated to optimize conditions. As shown in Figs. 4E–F and 6A–B, further increasing concentrations of Na_2SO_3 and KI from 50 and 10 mM to 100 and 20 mM, respectively, did not significantly change the photodegradation profiles of PFAS mixtures. Additionally, the overall deF% just increased slightly to 60.5 ± 2.8 % as the concentrations rose (Figs. 5 and 7). These findings were consistent with the similar PFAS photodegradation profiles observed when doubling the concentrations of Na_2SO_3 and KI from 50 and 10 mM, respectively, at the stable pH of 12, as shown in Fig. 6C–F. Interestingly, the overall deF% decreased from 66.5 ± 1.1 % to 59.9 ± 2.7 % as the concentrations increased (Fig. 7). These findings suggested that while both Na_2SO_3 and KI played a role in the photoreductive degradation of PFAS, there appeared to be a threshold beyond which additional increases in their concentrations did not significantly enhance the degradation efficiency. This plateau effect indicated that other factors, such as the saturation of reactive intermediates, mass transfer limitations, or the limitations imposed by the reaction kinetics, might be influencing the overall degradation process.

Furthermore, the role of pH control was examined to elucidate its influence on the photochemical degradation of PFAS, particularly in systems where e_{aq}^- play a crucial role. In the comparison of degradation at 50 mM Na_2SO_3 and 10 mM KI at an initial pH of 12 with and without pH stabilization, it was evident that maintaining a stable pH at 12 notably affected the degradation process (Figs. 6C–D and S6B),

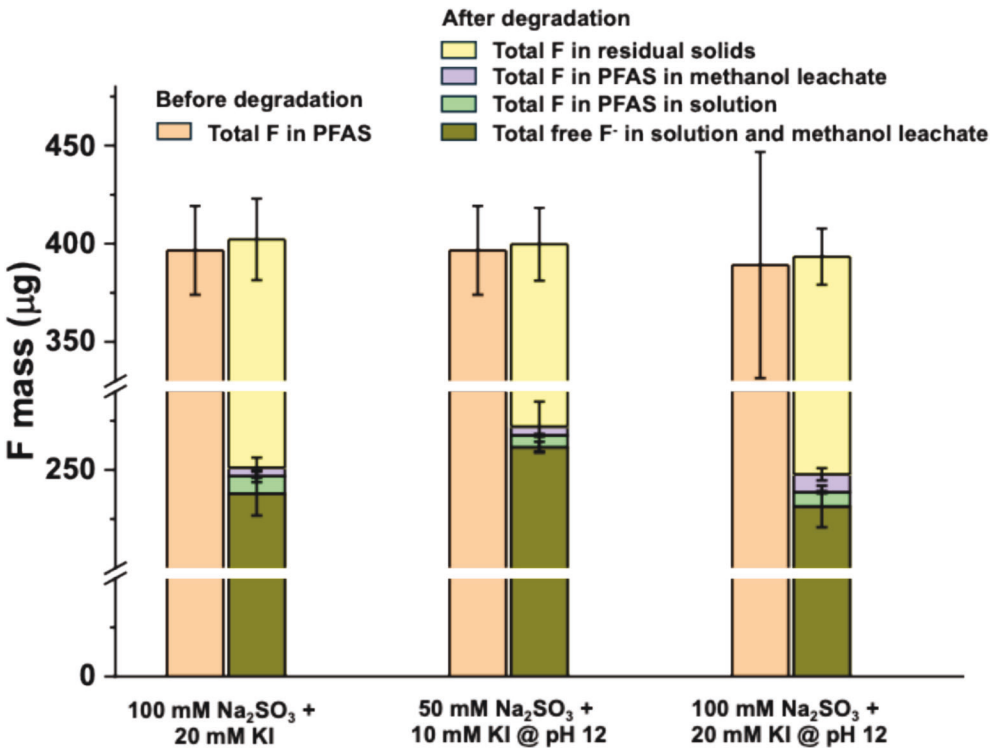

Fig. 8. Mass balance of fluorine before and after photodegradation of adsorbed PFAS in the spent MMC at various conditions: 100 mM Na_2SO_3 and 20 mM KI at initial pH 12 (uncontrolled), 50 mM Na_2SO_3 and 10 mM KI at stable pH 12, and 100 mM Na_2SO_3 and 20 mM KI at stable pH 12. The total initial adsorbed mass of PFAS was 3.1 mg/g, with each PFAS accounting for approximately the same amount. The spent MMC dose in aqueous solution was 2.5 g/L (0.2 g in 80 mL). Other chemical reagent and conditions for all groups were: 5 mM $NaHCO_3$ at around 20 °C. Error bars represent the standard deviations of duplicate tests. Statistical analyses showed no significant differences of total F mass before and after photodegradation.

compared to that without pH control which ended with a final pH of 9.6 ± 0.1 (Figs. 4E–F and S5C). This was attributed primarily to the increased availability of e^-_{aq}, as the high pH environment minimized the protonation of these reactive species, thereby preserving their concentration and reactivity [44,47]. Specifically, at a stable pH of 12, the lower consumption of e^-_{aq} by H^+ facilitated a more effective cleavage of strong C—F bonds in PFAS, leading to a higher overall deF% as shown in Figs. 5 and 7. The enhanced degradation can be ascribed to the more favorable conditions for nucleophilic attack by e^-_{aq}, which has been identified as the primary mechanism driving the reductive defluorination of PFAS, particularly for PFCAs [61].

However, when the reductant concentrations were elevated to 100 mM Na_2SO_3 and 20 mM KI, the effect of pH stabilization at 12 was less significant, as shown in Fig. 6A–B and E–F, as well as Fig. S6A and C. This was also consistent with the similar overall deF% between the two groups (Fig. 7). The reasons might be due to that at higher reductant concentrations, saturation of reactive species could be reached, which influenced the overall degradation efficiency [62], making the pH control less critical. Additionally, an excess of I^- can result in the formation of reactive iodine species, such as I_2, $I_2^{\bullet-}$, and I_3^-, which are potent scavengers of e^-_{aq} [29,63,64], thereby reducing the system's dependency on pH at higher reductant levels.

The mass balance of fluorine before and after photodegradation under the three different conditions was also investigated, as displayed in Fig. 8. All organofluorine and fluoride were derived from PFAS adsorbed to MMC, from which the theoretical total organofluorine was calculated. After photodegradation, the organofluorine could be in: (i) the parent and daughter PFAS in the aqueous solution; (ii) the same set of PFAS in the leachate of the residual MMC by basic methanol; (iii) the same set of PFAS in the MMC residual after methanol extraction. The organofluorine concentration in (i) and (ii) was calculated based on PFAS quantified in each stream. Those in (iii) were quantified by CIC which converts organofluorine to fluoride. Solutions from (i) and (ii) were also subjected to measurement of inorganic fluoride by a fluoride ion-selective electrode. The deF% was calculated by dividing the sum of all organofluorine from the three sources and inorganic fluoride from the two types of solution by the total theoretical organofluorine concentration. The CIC results showed that a significant fraction of non-extractable organofluorine was retained in the residual MMC for all three conditions. Interestingly, the presence of non-extractable PFAS in the residual MMC did not negatively affect the reusability of MMC (details in Section 3.5).

3.5. Regeneration and reuse of the MMC

Despite adsorption technique's extensive usage in PFAS removal, the difficulty of renewing these materials when their adsorption ability is depleted is a major limitation of their full-scale deployment. Restoring the adsorption capacity of the spent materials requires regeneration procedures that are both economically viable and environmentally secure, allowing for the virtually full removal of adsorbed PFAS [65]. Thus, additional tests were carried out on MMC to examine its possible reutilization following photochemical degradation. The tests measured adsorption efficiency at an initial concentration of 10 μg/L for each tested PFAS, with a dose of 100 mg/L of regenerated MMC administered under varying contact times (1, 4, 8, 24, and 48 h). The results showed that PFOA and 6:2 FTSA had a lower removal efficiency (around 70 %) with gradual desorption observed within 48 h, whereas PFHxA, PFDA, PFUnA, PFOS, and N-EtFOSAA exhibited nearly 100 % removal with no obvious desorption detected (Fig. 9A). These findings suggested that MMC could be regenerated by effective photodegradation of pre-concentrated PFAS, allowing for reuse without the need for further chemical regeneration. To comprehensively evaluate the reusability and durability of MMC, two additional photodegradation-adsorption cycles

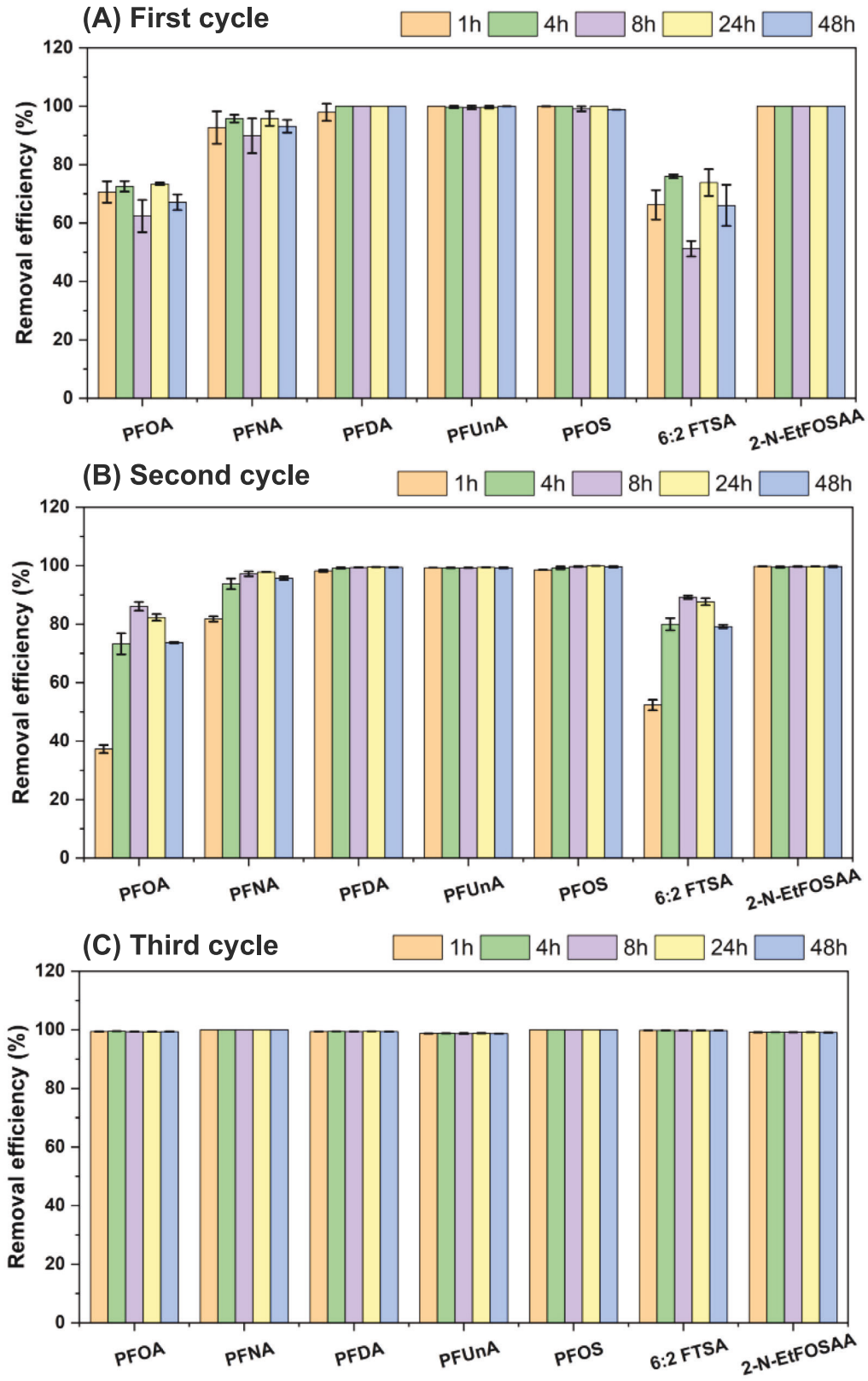

Fig. 9. Reuse of magnetic modified clay after photochemical degradation of the adsorbed PFAS at different contact times (1, 4, 8, 24, and 48 h) for three photodegradation-adsorption cycles: (A) first cycle, (B) second cycle, and (C) third cycle. The initial concentration of each tested PFAS was 10 μg/L, and the dose of regenerated MMC was 100 mg/L. The PFAS solution pH was unadjusted. Error bars represent the standard deviations of triplicate tests.

were conducted. The results demonstrated consistent regeneration performance, with the regenerated MMC maintaining its ability to remove PFAS effectively across all three cycles (Fig. 9). Notably, during the third cycle, all seven PFAS achieved nearly 100 % removal efficiency. This result indicated that the photodegradation process effectively continued to break down PFAS and fully restored the adsorption capacity of MMC, ensuring its sustained effectiveness across multiple cycles. These findings reinforced the potential of MMC as a practical and sustainable adsorbent, offering the distinct benefit of MMC compared to more traditional adsorbents such as AC or ion-exchange resins which requires either thermal or chemical regeneration, respectively. Aside from difficulties in regeneration, use of these conventional adsorbents needs to address the challenge of disposing properly the concentrated regenerant waste [66]. In future studies, density functional theory (DFT) and molecular dynamics simulations could be employed to gain a deeper theoretical understanding of degradation of PFAS in MMC and mechanisms for regeneration, offering valuable insights into the molecular interactions and energy barriers involved.

4. Conclusions

This study explored the effectiveness of the combined adsorption by MMC and destruction of the adsorbed PFAS by photodegradation. The results underscored MMC's high efficiency in PFAS adsorption, achieving near-complete adsorption of the six regulated PFAS within 48 h. Under UV light, a significant photoreductive degradation of PFAS adsorbed onto MMC was observed, leading to notable reductions in the concentrations of various PFAS species. Results indicated both reductant concentrations and pH affected the defluorination of PFAS with the optimal conditions of 50 mM Na_2SO_3 and 10 mM KI at stable pH 12. Post photodegradation, the MMC demonstrated potential for reuse for multiple photodegradation-adsorption cycles. In conclusion, MMC could be a promising material for removing PFAS in water. The effective photodegradation could lead to ways for adsorbent regeneration and reuse.

CRediT authorship contribution statement

Tao Jiang: Writing – review & editing, Writing – original draft, Visualization, Validation, Methodology, Investigation, Formal analysis, Data curation, Conceptualization. **Md. Nahid Pervez:** Writing – original draft, Investigation, Formal analysis. **Aswin Kumar Ilango:** Writing – review & editing, Visualization, Investigation. **Yanna Liang:** Writing – review & editing, Validation, Supervision, Investigation, Funding acquisition, Formal analysis, Conceptualization.

Declaration of competing interest

The authors declare that they have no known competing financial interests or personal relationships that could have appeared to influence the work reported in this paper.

Acknowledgments

The authors acknowledge financial supports from the U.S. National Science Foundation under award number CBET 2225596, FuzeHub Jeff Lawrence Innovation Fund (project number 2022-IC-0000000076), and the Technology Accelerator Fund from State University of New York to YL.

Appendix A. Supplementary data

Supplementary data to this article can be found online at https://doi.org/10.1016/j.jwpe.2024.106733.

Data availability

Data will be made available on request.

References

[1] P.M. Murphy, T. Hewat, Fluorosurfactants in enhanced oil recovery, Open Pet. Eng. J. 1 (1) (2008).
[2] Y. Meng, Y. Yao, H. Chen, Q. Li, H. Sun, Legacy and emerging per-and polyfluoroalkyl substances (PFASs) in Dagang Oilfield: multimedia distribution and contributions of unknown precursors, J. Hazard. Mater. 412 (2021) 125177.
[3] X. Trier, K. Granby, J.H. Christensen, Polyfluorinated surfactants (PFS) in paper and board coatings for food packaging, Environ. Sci. Pollut. Res. 18 (7) (2011) 1108–1120.
[4] S. Schellenberger, I. Liagkouridis, R. Awad, S. Khan, M. Plassmann, G. Peters, J. P. Benskin, I.T. Cousins, An outdoor aging study to investigate the release of per-and polyfluoroalkyl substances (PFAS) from functional textiles, Environ. Sci. Technol. 56 (6) (2022) 3471–3479.
[5] X. Dauchy, V. Boiteux, C. Bach, C. Rosin, J.F. Munoz, Per-and polyfluoroalkyl substances in firefighting foam concentrates and water samples collected near sites impacted by the use of these foams, Chemosphere 183 (2017) 53–61.
[6] D.B. Leary, M. Takazawa, K. Kannan, N. Khalil, Perfluoroalkyl substances and metabolic syndrome in firefighters: a pilot study, J. Occup. Environ. Med. 62 (1) (2020) 52–57.
[7] Y. Fujii, K.H. Harada, A. Koizumi, Occurrence of perfluorinated carboxylic acids (PFCAs) in personal care products and compounding agents, Chemosphere 93 (3) (2013) 538–544.
[8] M. Kotthoff, J. Müller, H. Jürling, M. Schlummer, D. Fiedler, Perfluoroalkyl and polyfluoroalkyl substances in consumer products, Environ. Sci. Pollut. Res. 22 (19) (2015) 14546–14559.
[9] J. Glüge, M. Scheringer, I.T. Cousins, J.C. DeWitt, G. Goldenman, D. Herzke, R. Lohmann, C.A. Ng, X. Trier, Z. Wang, An overview of the uses of per-and polyfluoroalkyl substances (PFAS), Environ. Sci.: Process. Impacts 22 (12) (2020) 2345–2373.
[10] M.N. Ehsan, M. Riza, M.N. Pervez, Y. Liang, Source identification and distribution of per- and polyfluoroalkyl substances (PFAS) in the freshwater environment of USA, Int. J. Environ. Sci. Technol. (2024), https://doi.org/10.1007/s13762-024-05851-x.
[11] M.N. Pervez, T. Jiang, J.K. Mahato, A.K. Ilango, Y. Kumaran, Y. Zuo, W. Zhang, H. Efstathiadis, J.I. Feldblyum, M.V. Yigit, Y. Liang, Surface modification of graphene oxide for fast removal of per- and polyfluoroalkyl substances (PFAS) mixtures from river water, ACS ES&T Water 4 (7) (2024) 2968–2980.
[12] S.C.E. Leung, P. Shukla, D. Chen, E. Eftekhari, H. An, F. Zare, N. Ghasemi, D. Zhang, N.T. Nguyen, Q. Li, Emerging technologies for PFOS/PFOA degradation: a review, Sci. Total Environ. 827 (2022) 153669.
[13] M. Sörengård, E. Östblom, S. Köhler, L. Ahrens, Adsorption behavior of per-and polyfluoralkyl substances (PFASs) to 44 inorganic and organic sorbents and use of dyes as proxies for PFAS sorption, J. Environ. Chem. Eng. 8 (3) (2020) 103744.
[14] A.K. Ilango, T. Jiang, W. Zhang, M.N. Pervez, J.I. Feldblyum, H. Efstathiadis, Y. Liang, Enhanced adsorption of mixtures of per- and polyfluoroalkyl substances in water by chemically modified activated carbon, ACS ES&T Water 3 (11) (2023) 3708–3715.
[15] T.H. Boyer, Y. Fang, A. Ellis, R. Dietz, Y.J. Choi, C.E. Schaefer, C.P. Higgins, T. J. Strathmann, Anion exchange resin removal of per-and polyfluoroalkyl substances (PFAS) from impacted water: a critical review, Water Res. 200 (2021) 117244.
[16] F. Dixit, R. Dutta, B. Barbeau, P. Berube, M. Mohseni, PFAS removal by ion exchange resins: a review, Chemosphere 272 (2021) 129777.
[17] X. Chen, X. Xia, X. Wang, J. Qiao, H. Chen, A comparative study on sorption of perfluorooctane sulfonate (PFOS) by chars, ash and carbon nanotubes, Chemosphere 83 (10) (2011) 1313–1319.
[18] Q. Zhang, S. Deng, G. Yu, J. Huang, Removal of perfluorooctane sulfonate from aqueous solution by crosslinked chitosan beads: sorption kinetics and uptake mechanism, Bioresour. Technol. 102 (3) (2011) 2265–2271.
[19] A.K. Ilango, T. Jiang, W. Zhang, J.I. Feldblyum, H. Efstathiadis, Y. Liang, Surface-modified biopolymers for removing mixtures of per-and polyfluoroalkyl substances from water: screening and removal mechanisms, Environ. Pollut. 331 (2023) 121865.
[20] A.K. Ilango, P. Arathala, R.A. Musah, Y. Liang, Experimental and density functional theory investigation of surface-modified biopolymer for improved adsorption of mixtures of per- and polyfluoroalkyl substances in water, Water Res. 255 (2024) 121458.
[21] T. Jiang, W. Zhang, A.K. Ilango, J.I. Feldblyum, Z. Wei, H. Efstathiadis, M.V. Yigit, Y. Liang, Surfactant-modified clay for adsorption of mixtures of per-and polyfluoroalkyl substances (PFAS) in aqueous solutions, ACS Appl. Eng. Mater. 1 (1) (2023) 394–407.
[22] T. Jiang, M.N. Pervez, A.K. Ilango, Y.K. Ravi, W. Zhang, J.I. Feldblyum, M.V. Yigit, H. Efstathiadis, Y. Liang, Magnetic surfactant-modified clay for enhanced adsorption of mixtures of per- and polyfluoroalkyl substances (PFAS) in snowmelt: improving practical applicability and efficiency, J. Hazard. Mater. 471 (2024) 134390.
[23] Y. Zhang, A. Thomas, O. Apul, A.K. Venkatesan, Coexisting ions and long-chain per-and polyfluoroalkyl substances (PFAS) inhibit the adsorption of short-chain PFAS by granular activated carbon, J. Hazard. Mater. 460 (2023) 132378.

[24] J.-L. Lim, M. Okada, Regeneration of granular activated carbon using ultrasound, Ultrason. Sonochem. 12 (4) (2005) 277–282.
[25] A. Larasati, G.D. Fowler, N.J. Graham, Chemical regeneration of granular activated carbon: preliminary evaluation of alternative regenerant solutions, Environ. Sci.: Water Res. Technol. 6 (8) (2020) 2043–2056.
[26] R.V. McQuillan, G.W. Stevens, K.A. Mumford, The electrochemical regeneration of granular activated carbons: a review, J. Hazard. Mater. 355 (2018) 34–49.
[27] B. Sonmez Baghirzade, Y. Zhang, J.F. Reuther, N.B. Saleh, A.K. Venkatesan, O. G. Apul, Thermal regeneration of spent granular activated carbon presents an opportunity to break the forever PFAS cycle, Environ. Sci. Technol. 55 (9) (2021) 5608–5619.
[28] S. Verma, B. Mezgebe, C.A. Hejase, E. Sahle-Demessie, M.N. Nadagouda, Photodegradation and photocatalysis of per- and polyfluoroalkyl substances (PFAS): a review of recent progress, Next Mater. 2 (2024) 100077.
[29] Z. Liu, Z. Chen, J. Gao, Y. Yu, Y. Men, C. Gu, J. Liu, Accelerated degradation of perfluorosulfonates and perfluorocarboxylates by UV/sulfite + iodide: reaction mechanisms and system efficiencies, Environ. Sci. Technol. 56 (6) (2022) 3699–3709.
[30] M. Gar Alalm, D.C. Boffito, Mechanisms and pathways of PFAS degradation by advanced oxidation and reduction processes: a critical review, Chem. Eng. J. 450 (2022) 138352.
[31] M. Mirabediny, J. Sun, T.T. Yu, B. Åkermark, B. Das, N. Kumar, Effective PFAS degradation by electrochemical oxidation methods-recent progress and requirement, Chemosphere 321 (2023) 138109.
[32] Z. Song, X. Dong, N. Wang, L. Zhu, Z. Luo, J. Fang, C. Xiong, Efficient photocatalytic defluorination of perfluorooctanoic acid over BiOCl nanosheets via a hole direct oxidation mechanism, Chem. Eng. J. 317 (2017) 925–934.
[33] L. Duan, B. Wang, K. Heck, S. Guo, C.A. Clark, J. Arredondo, M. Wang, T.P. Senftle, P. Westerhoff, X. Wen, Y. Song, Efficient photocatalytic PFOA degradation over boron nitride, Environ. Sci. Technol. Lett. 7 (8) (2020) 613–619.
[34] X. Liu, W. Wei, J. Xu, D. Wang, L. Song, B.J. Ni, Photochemical decomposition of perfluorochemicals in contaminated water, Water Res. 186 (2020) 116311.
[35] C.D. Vecitis, H. Park, J. Cheng, B.T. Mader, M.R. Hoffmann, Treatment technologies for aqueous perfluorooctanesulfonate (PFOS) and perfluorooctanoate (PFOA), Front. Environ. Sci. Eng. China 3 (2) (2009) 129–151.
[36] H. Javed, C. Lyu, R. Sun, D. Zhang, P.J. Alvarez, Discerning the inefficacy of hydroxyl radicals during perfluorooctanoic acid degradation, Chemosphere 247 (2020) 125883.
[37] F. Liu, X. Guan, F. Xiao, Photodegradation of per- and polyfluoroalkyl substances in water: a review of fundamentals and applications, J. Hazard. Mater. 439 (2022) 129580.
[38] H. Tian, Y. Guo, B. Pan, C. Gu, H. Li, S.A. Boyd, Enhanced photoreduction of nitro-aromatic compounds by hydrated electrons derived from indole on natural montmorillonite, Environ. Sci. Technol. 49 (13) (2015) 7784–7792.
[39] L. Yang, L. He, J. Xue, Y. Ma, Z. Xie, L. Wu, M. Huang, Z. Zhang, Persulfate-based degradation of perfluorooctanoic acid (PFOA) and perfluorooctane sulfonate (PFOS) in aqueous solution: review on influences, mechanisms and prospective, J. Hazard. Mater. 393 (2020) 122405.
[40] J. Jortner, M. Ottolenghi, G. Stein, On the photochemistry of aqueous solutions of chloride, bromide, and iodide ions, J. Phys. Chem. 68 (2) (1964) 247–255.
[41] E. Banayan Esfahani, F.A. Zeidabadi, S. Zhang, M. Mohseni, Photo-chemical/catalytic oxidative/reductive decomposition of per- and poly-fluoroalkyl substances (PFAS), decomposition mechanisms and effects of key factors: a review, Environ. Sci.: Water Res. Technol. 8 (4) (2022) 698–728.
[42] J. Cui, P. Gao, Y. Deng, Destruction of per- and polyfluoroalkyl substances (PFAS) with advanced reduction processes (ARPs): a critical review, Environ. Sci. Technol. 54 (7) (2020) 3752–3766.
[43] Y. Qu, C. Zhang, F. Li, J. Chen, Q. Zhou, Photo-reductive defluorination of perfluorooctanoic acid in water, Water Res. 44 (9) (2010) 2939–2947.
[44] M.J. Bentel, Z. Liu, Y. Yu, J. Gao, Y. Men, J. Liu, Enhanced degradation of perfluorocarboxylic acids (PFCAs) by UV/sulfite treatment: reaction mechanisms and system efficiencies at pH 12, Environ. Sci. Technol. Lett. 7 (5) (2020) 351–357.
[45] Y. Gu, W. Dong, C. Luo, T. Liu, Efficient reductive decomposition of perfluorooctanesulfonate in a high photon flux UV/sulfite system, Environ. Sci. Technol. 50 (19) (2016) 10554–10561.
[46] R. Tenorio, J. Liu, X. Xiao, A. Maizel, C.P. Higgins, Destruction of per- and polyfluoroalkyl substances (PFASs) in aqueous film-forming foam (AFFF) with UV-sulfite photoreductive treatment, Environ. Sci. Technol. 54 (11) (2020) 6957–6967.
[47] Z. Liu, Y. Yu, C. Ren, J. Gao, V.F. Pulikkal, M. Sun, Y. Men, J. Liu, Near-quantitative defluorination of perfluorinated and fluorotelomer carboxylates and sulfonates with integrated oxidation and reduction, Environ. Sci. Technol. 55 (10) (2021) 7052–7062.
[48] K. Kabra, R. Chaudhary, R.L. Sawhney, Treatment of hazardous organic and inorganic compounds through aqueous-phase photocatalysis: a review, Ind. Eng. Chem. Res. 43 (24) (2004) 7683–7696.
[49] A. Kugler, H. Dong, C. Li, C. Gu, C.E. Schaefer, Y.J. Choi, D. Tran, M. Spraul, C. P. Higgins, Reductive defluorination of perfluorooctanesulfonic acid (PFOS) by hydrated electrons generated upon UV irradiation of 3-indole-acetic-acid in 12-aminolauric-modified montmorillonite, Water Res. 200 (2021) 117221.
[50] X. Xu, W. Chen, S. Zong, X. Ren, D. Liu, Magnetic clay as catalyst applied to organics degradation in a combined adsorption and Fenton-like process, Chem. Eng. J. 373 (2019) 140–149.
[51] M.K. Acar, T. Altun, I.H. Gubbuk, Synthesis and characterization of silver doped magnetic clay nanocomposite for environmental applications through effective RhB degradation, Int. J. Environ. Sci. Technol. 20 (4) (2023) 4219–4234.
[52] W. Zhang, T. Jiang, Y. Liang, Stabilization of per-and polyfluoroalkyl substances (PFAS) in sewage sludge using different sorbents, J. Hazard. Mater. Adv. 6 (2022) 100089.
[53] T. Jiang, W. Zhang, Y. Liang, Uptake of individual and mixed per-and polyfluoroalkyl substances (PFAS) by soybean and their effects on functional genes related to nitrification, denitrification, and nitrogen fixation, Sci. Total Environ. 838 (2022) 156640.
[54] W. Zhang, Y. Liang, Performance of different sorbents toward stabilizing per-and polyfluoroalkyl substances (PFAS) in soil, Environ. Adv. 8 (2022) 100217.
[55] T. Jiang, M.N. Pervez, M.M. Quianes, W. Zhang, V. Naddeo, Y. Liang, Effective stabilization of per-and polyfluoroalkyl substances (PFAS) precursors in wastewater treatment sludge by surfactant-modified clay, Chemosphere 341 (2023) 140081.
[56] R. Aro, U. Eriksson, A. Kärrman, I. Reber, L.W. Yeung, Combustion ion chromatography for extractable organofluorine analysis, iScience 24 (9) (2021).
[57] M.J. Bentel, Y. Yu, L. Xu, Z. Li, B.M. Wong, Y. Men, J. Liu, Defluorination of per-and polyfluoroalkyl substances (PFASs) with hydrated electrons: structural dependence and implications to PFAS remediation and management, Environ. Sci. Technol. 53 (7) (2019) 3718–3728.
[58] Z. Chen, H. Tian, H. Li, J. Li, R. Hong, F. Sheng, C. Wang, C. Gu, Application of surfactant modified montmorillonite with different conformation for photo-treatment of perfluorooctanoic acid by hydrated electrons, Chemosphere 235 (2019) 1180–1188.
[59] J. Wen, H. Li, L.D.M. Ottosen, J. Lundqvist, L. Vergeynst, Comparison of the photocatalytic degradability of PFOA, PFOS and GenX using Fe-zeolite in water, Chemosphere 344 (2023) 140344.
[60] E.B. Esfahani, F.A. Zeidabadi, M. Jafarikojour, M. Mohseni, Photo-oxidative/reductive decomposition of perfluorooctanoic acid (PFOA) and its common alternatives: mechanism and kinetic modeling, J. Water Proc. Eng. 61 (2024) 105332.
[61] Z. Cheng, Q. Chen, Z. Liu, J. Liu, Y. Liu, S. Liu, X. Gao, Y. Tan, Z. Shen, Interpretation of reductive PFAS defluorination with quantum chemical parameters, Environ. Sci. Technol. Lett. 8 (8) (2021) 645–650.
[62] Y. Li, Y. Jiang, X. Liu, Q. Bai, H. Liu, J. Wang, P. Zhang, L. Lu, X. Yuan, Influence of reactive oxygen species concentration and ambient temperature on the evolution of chemical bonds during plasma cleaning: a molecular dynamics simulation, RSC Adv. 12 (47) (2022) 30754–30763.
[63] H. Park, C.D. Vecitis, J. Cheng, N.F. Dalleska, B.T. Mader, M.R. Hoffmann, Reductive degradation of perfluoroalkyl compounds with aquated electrons generated from iodide photolysis at 254 nm, Photochem. Photobiol. Sci. 10 (12) (2011) 1945–1953.
[64] H. Park, C.D. Vecitis, J. Cheng, W. Choi, B.T. Mader, M.R. Hoffmann, Reductive defluorination of aqueous perfluorinated alkyl surfactants: effects of ionic headgroup and chain length, Chem. A Eur. J. 113 (4) (2009) 690–696.
[65] E. Gagliano, M. Sgroi, P.P. Falciglia, F.G. Vagliasindi, P. Roccaro, Removal of poly-and perfluoroalkyl substances (PFAS) from water by adsorption: role of PFAS chain length, effect of organic matter and challenges in adsorbent regeneration, Water Res. 171 (2020) 115381.
[66] X. Fang, L. Jin, X. Sun, H. Huang, Y. Wang, H. Ren, A data-driven analysis to discover research hotspots and trends of technologies for PFAS removal, Environ. Res. 251 (2024) 118678.